ChemComm

COMMUNICATION

View Article Online
View Journal | View Issue

Cite this: *Chem. Commun.*, 2022, 58, 3310

Received 9th January 2022,
Accepted 14th February 2022

DOI: 10.1039/d2cc00151a

rsc.li/chemcomm

Self-supported amorphous $TaN_x(O_y)$/nickel foam thin film as an advanced electrocatalyst for hydrogen evolution reaction†

Ganesh Babu Thiyagarajan,[ab] Raghunath Sharma Mukkavilli,[a] David Graf,[c] Thomas Fischer,[c] Michael Wilhelm,[c] Silke Christiansen,[de] Sanjay Mathur *[ac] and Ravi Kumar *[ab]

Chemical vapor deposited (CVD) amorphous tantalum-oxy nitride film on porous three-dimensional (3D) nickel foam ($TaN_x(O_y)$/NF) utilizing tantalum precursor, tris(diethylamino)(ethylimino)tantalum(V), ([Ta(NEt)(NEt$_2$)$_3$]) with preformed Ta–N bonds is reported as a potential self-supported electrocatalyst for hydrogen evolution reaction (HER). The morphological analyses revealed the formation of thin film of core–shell structured $TaN_x(O_y)$ coating (*ca.* 236 nm) on NF. In 0.5 M H_2SO_4, $TaN_x(O_y)$/NF exhibited enhanced HER activity with a low onset potential as compared to the bare NF (−50 mV *vs.* −166 mV). The $TaN_x(O_y)$/NF samples also displayed higher current density (−11.08 mA cm^{-2} *vs.* −3.36 mA cm^{-2} at 400 mV), lower Tafel slope (151 mV dec^{-1} *vs.* 179 mV dec^{-1}) and lower charge transfer resistance exemplifying the advantage of $TaN_x(O_y)$ coating towards enhanced HER performance. The enhanced HER catalytic activity is attributed to the synergistic effect between the amorphous $TaN_x(O_y)$ film and the nickel foam.

Nanostructuring earth abundant electrocatalysts with catalytic activity on par with the current state of the art materials like platinum, albeit at a much lower cost and an enhanced stability is a key strategy in envisaging a future of clean and renewable energy production.[1,2] Among the various earth abundant electrocatalysts, transition metal nitrides have garnered a lot of attention as Pt free hydrogen evolution reaction (HER) electrocatalysts owing to their superior properties such as stability in acidic medium, and Pt like electronic behavior.[3,4] Further, theoretical calculations on metal nitride surfaces have identified Ta–N as a potential electrocatalyst for HER based on its low overpotential compared to other nitrides (Sc, Ti, Y, Hf). Also, these nitrides demonstrated activation energies for Tafel reaction (hydrogen adsorption) on par with elemental Pt- the current state of the art material for HER with no ammonia evolution.[5] However, few studies have experimentally realized this. For instance, Alhajri *et al.*, using mesoporous carbon nitride as template, successfully demonstrated a TaN phase that delivered hydrogen at an over potential as low as 160 mV.[6] Also, in a recent study, porous Ta_5N_6 single crystal demonstrated electrocatalytic hydrogen evolution behavior on par with MoS_2.[7] However, most of these reports are centered around studying the electrocatalytic behavior *via* the cumbersome process of catalytic ink preparation, which involves multiple optimization steps, use of expensive polymer binders and also suffer from poor catalyst adhesion and subsequent ohmic losses.[8] In contrast, self-supported electrocatalysts wherein porous nanoarchitectures of active material is directly coated/grown on a porous conducting substrate with conformal control and uniformity circumvents the issues[9–11] One such methodology that enables growth of a uniform and conformal thin film on any substrate can be envisaged through chemical vapor deposition (CVD).[12] In this study, nickel foams (NF) have been selected as porous 3D conducting substrates, which have originally been used as electrode-support in batteries and as supports in water electrolysis.[13,14] Also, interfacing the catalyst with Ni was found to enhance hydrogen evolution kinetics by decreasing the hydrogen adsorption barrier.[14,15] For instance, when cobalt nitride (Co_2N) was interfaced with Ni, enhanced electron transfer combined with lowering of Gibbs adsorption free energy was observed by virtue of a synergistic effect.[16,17] Further, amorphous nanostructures by virtue of their intrinsic disorder and unsaturated bonds provide enhanced number of active sites for electrocatalysis.[18] In this study, a multi-pronged strategy was adopted to develop an advanced electrocatalyst for HER: (1) Based on theoretical studies and promising stability,[19]

[a] *Laboratory for High Performance Ceramics, Department of Metallurgical and Materials Engineering, Indian Institute of Technology-Madras (IIT Madras), Chennai 600036, India. E-mail: nvrk@iitm.ac.in*
[b] *Ceramic Technologies Group-Center of Excellence in Materials and Manufacturing for Futuristic Mobility, Indian Institute of Technology-Madras (IIT Madras), Chennai 600036, India*
[c] *Department of Chemistry, Institute of Inorganic Chemistry, University of Cologne, Greinstraße 6, 50939 Cologne, Germany. E-mail: mathurs@uni-koeln.de*
[d] *Department Correlative Microscopy and Materials Data, Fraunhofer Institute for Ceramic Technologies and Systems (IKTS), Forchheim, Germany*
[e] *Physics Department, Freie Universität Berlin (FU), Berlin, Germany*

† Electronic supplementary information (ESI) available. See DOI: 10.1039/d2cc00151a

Ta–N was chosen as the active catalyst (2) A precursor with preformed Ta–N bonds was synthesized to avoid any cumbersome high temperature ammonia pyrolysis (3) the precursor was later pyrolyzed at low temperatures (500 °C) to retain an amorphous structure (4) Nickel foam was selected as the substrate both for its self-supporting role and also to create interfaces with the amorphous TaN_x layer. Herein, we report for the first time, facile, direct growth of tantalum-based nitride on NF *via.* CVD for HER applications.

Initially, $[Ta(NEt)(NEt_2)_3]$ precursor was synthesized *via.* three step reaction as per the previously reported procedure[20] (For further information, ref. S1 and S2 ESI†). ^1H and ^{13}C-NMR spectrum shows no evidence for the formation of pentakis(diethylamido)tantalum $[Ta(NEt_2)_5]$ which was reported by Bradley *et al.*[20] [Fig. S1(a and b), ESI†]. On the other hand, $[Ta(NEt)(NEt_2)_3]$ is made of mixture of ethylimidotris(diethylamido)tantalum and ethyl-iminoethyltris(diethylamido)tantalum complexes.[21] ^1H NMR shows the signal at δ = 4.23 ppm (q) corresponding to $CH_3CH(N)Ta$ group which suggests the presence of an asymmetric center in the complex, namely ethyl-iminoethyltris(diethylamido)tantalum [Fig. S1(a), ESI†]. The formation of the asymmetric centered complex was further confirmed by ^{13}C NMR spectra [Fig. S1(b), ESI†], which shows a strong chemical shift at 63.34 ppm proving beyond doubt that the reaction of diethylamine with $TaCl_5$ gives mixture of ethylimidotris(diethylamido)tantalum and ethyl-iminoethyltris(diethylamido)tantalum complexes *via* S_N2 mechanism [Fig. S1(c), ESI†].

Thermogravimetric analysis and its derivatives of the precursor up to 800 °C under N_2 atmosphere were shown in Fig. S1(d) (ESI†). The precursor showed a two-stage weight loss with early decomposition, starting at 40 °C (initial decomposition temperature, T_i) and continues up to 310 °C (final decomposition temperature, T_f) leading to a lower ceramic yield of 25 wt. % at 800 °C. The low ceramic yield is due to evaporation of lower molecular weight organic compounds before the ceramization process. The two-stage decomposition is due to the transformation of ethyl-iminoethyl tris(diethylamido) tantalum to ethylimido tris(diethylamido) tantalum complex. The boiling points of these two complexes were close and hence could not be separated completely by distillation process. On the other hand, elimination of one equivalent of ethylene from ethylimidotris(diethylamido)tantalum at temperatures exceeding 200 °C to form ethyl-iminoethyltris(diethylamido)tantalum complex was a known process.[22] Since thin films used to be deposited at much higher temperatures (500 °C), ethyl-iminoethyl tris(diethylamido) tantalum complex will be completely transformed into ethylimido tris(diethylamido) tantalum complex before it could be deposited into thin films.

$[Ta(NEt)(NEt_2)_3]$ precursors were then introduced into a horizontal cold-wall CVD reactor through a glass tube by applying a ultra-high vacuum (10^{-6} mbar) and heating the precursor reservoir to the 120 °C. The coatings were obtained on a 3D nickel foam (2×3 cm^2) placed on an inductively heated graphite susceptor (500 °C) and designated as $TaN_x(O_y)$/NF. A uniform coating of $TaN_x(O_y)$ on NF with an average thickness of 236 nm [Fig. 1(a–e)] is observed. The mapping shows that Ta, N, Ni is homogeneously distributed on the NF confirming the conformal coating by CVD technique [Fig. 1(f)]. Moreover, the mapping also shows the presence a non-uniform distribution of and oxygen as contaminations at the surface. The presence of oxygen is possibly due to the oxidation of TaN phase in the ambient after deposition by CVD.

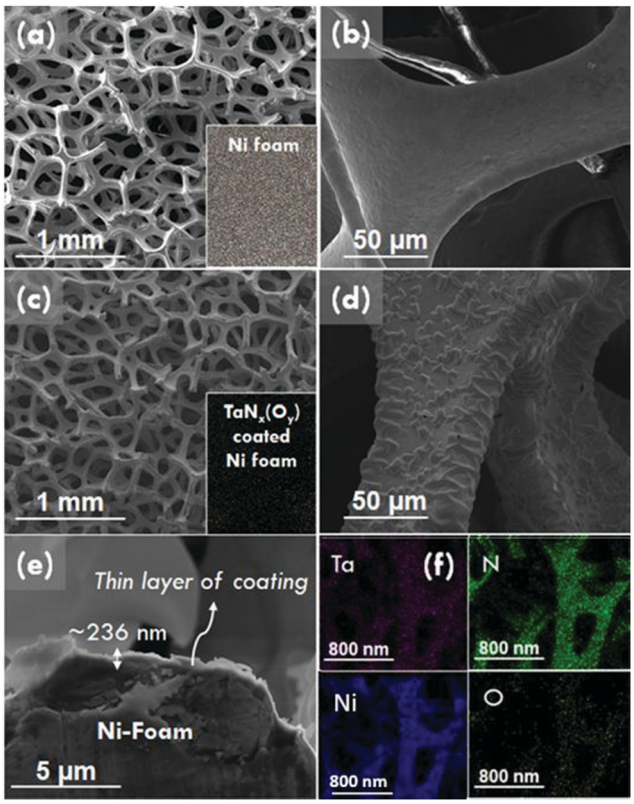

Fig. 1 SEM image of bare NF [(a) and (b)], $TaN_x(O_y)$/NF [(c) and (d)], (e) cross-sectional SEM image of $TaN_x(O_y)$/NF and (f) Elemental distribution mapping of $TaN_x(O_y)$/NF. The inset of Fig. (a and c) shows the photographic image of bare NF and $TaN_x(O_y)$/NF exemplifying a clear difference in color after the deposition of $TaN_x(O_y)$ on NF, respectively.

The XPS analysis substantiate the formation of TaN_x film on NF substrate [Fig. 2(a)]. Ta 4f and 5p peak was deconvoluted into a set of doublets with a splitting of ~1.9 eV and ratio of ~0.75. The Ta peaks at 25.70 eV ($4f_{7/2}$), 25.60 eV ($4f_{5/2}$), 34.75 eV ($5p_{3/2}$), and 36.87 eV ($5p_{1/2}$) correspond to +5 oxidation state of Ta species in Ta_3N_5 phase on the surface[23] [Fig. 2(b)]. Further the atomic ratio of Ta:N was determined to be 0.54 correlating with the formation of Ta_3N_5 phase (Ta:N ratio 0.6). Also, the N 1s peak at 397 eV indicated the presence of a Ta–N bond [Fig. 2(c)]. It is also well known that the surface of TaN is unstable and rapidly oxidizes in contact with air to form Ta_2O_5 and Ta_3N_5 phases,[24,25] this was also reflected in O 1S peak at 530.32 eV indicating the presence of lattice oxygen (Ta_2O_5) [Fig. 2(d)].

HRTEM images further indicate that Ni grains are coated with an ultra-thin TaO_xN_y film (4 nm) due to rapid oxidation of as synthesized TaN film (Fig. S2, ESI†). Fig. 3(a) shows the linear sweep voltammograms (LSV) of bare NF and $TaN_x(O_y)$/NF

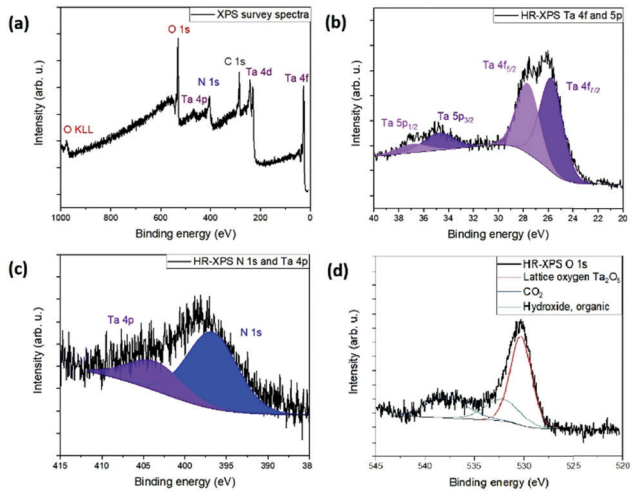

Fig. 2 (a) XPS survey spectrum of $TaN_x(O_y)$/NF, (b) HR XPS spectra of O 1s (c) HR XPS spectra of Ta 4f and Ta 5p and (d) HR XPS spectra of N 1s and Ta 4p.

in acidic (0.5 M H_2SO_4) electrolyte at a potential sweep rate of 5 mV s^{-1}. The onset potential for HER of NF electrode is found to be around *ca.* −0.16 V and a current density of 3 mA cm^2 (geometrical) is attained at an overpotential (η) value of 0.4 V. Whereas in the case of $TaN_x(O_y)$/NF, the onset potential is found to be *ca.* −50 mV and at η = 0.4 V has exemplified a high current density of 11 mA cm^{-2}, indicating better hydrogen evolution capability as compared to bare NF. The onset potential values are compared with the reported literature and are given in Table S1 (ESI†). $TaN_x(O_y)$/NF exhibits lower onset potential demonstrating higher HER activity.

The Tafel slope obtained for bare NF is 179 mV dec^{-1} [Fig. 3(b)], which is near to the theoretical Tafel slope of hydrogen adsorption to the active site, Volmer reaction (120 mV dec^{-1}).[26,27] The higher value observed in this case might be because of the parallel Ni oxide reduction occurring during HER considering that the equilibrium potential for Ni^{2+} to Ni^0 transition is −0.246 V vs RHE. The Tafel slope for $TaN_x(O_y)$/NF is 151 mV dec^{-1} and is attributed to the Volmer–Heyrovsky step. A lower slope value indicates a better reaction kinetics and a more active catalyst. Fig. 3(c) shows the Nyquist plot which depicts electrode–electrolyte interface behaviour and the Impedance parameters calculated from the equivalent circuit is given Table S2 (ESI†). The charge transfer resistance R_{ct} was lowered from 2.3 Ω to 0.9 Ω post TaN_xO_y coating. Concomitantly, a lower R_{mt} suggests better mass transport characteristics resulting in efficient transport of reactant to active sites aiding better HER activity. It is also to be noted that, $TaN_x(O_y)$/NF exemplified higher double layer capacitance (C_{dl}, 1.6 mF $s^{(a1-1)}$ *vs.* 1.1 mF $s^{(a2-1)}$, $a1$ = 0.75, $a2$ = 0.81) as determined from CPE_{dl}. C_{dl} can be taken as a measure of electrochemical surface area available for the catalytic reactions.[28] The higher C_{dl} of $TaN_x(O_y)$/NF is ascribed to increase in surface area because of the surface roughness as exemplified by SEM micrographs [Fig. 1(c and d)].

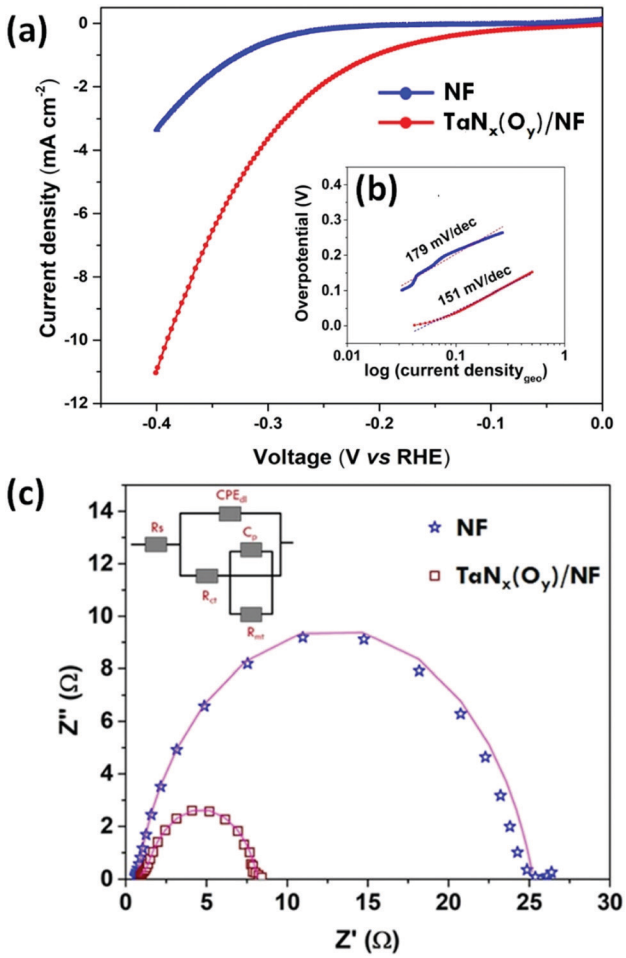

Fig. 3 (a) LSV of bare NF and $TaN_x(O_y)$/NF in 0.5 M H_2SO_4 at a potential sweep rate of 5 mV s^{-1} and (b) (inset) Tafel plots derived from the voltammograms (c) Nyquist plots of NF and $TaN_x(O_y)$/NF electrode. The inset shows the equivalent circuit to fit the plots, where R, CPE and C represent resistance, constant phase element and capacitor, respectively.

The Sabatier principle states that to achieve high HER reaction rates, the interaction of catalyst with the adsorbate (water molecules) should be neither too strong, nor too weak to facilitate hydrogen evolution.[29] It is to be noted that, tantalum possess weak adsorption capability of water molecules and strong desorption capability of hydrogen; whereas Ni exhibits strong adsorption of water molecules and weak desorption of hydrogen.[30] Hence, $TaN_x(O_y)$ coated NF possess the synergistic combination of Ta and Ni, where NF boosts the Volmer reaction (VR) aiding formation of adsorbed hydrogen (H*), whereas $TaN_x(O_y)$ facilitates Volmer–Heyrovsky reaction (VHR) leading to facile hydrogen evolution as shown in Fig. 4. Further, by virtue of its tendency to get readily oxidized, not many reports exist for Ta–N phases purely as hydrogen evolution electrocatalysts. However, as our study exemplifies, when interfaced with metals like Ni, Ta–N system can also deliver enhanced performance and coupled with their superior stability in highly acidic medium, these phases can in fact serve as better earth abundant electrocatalysts.

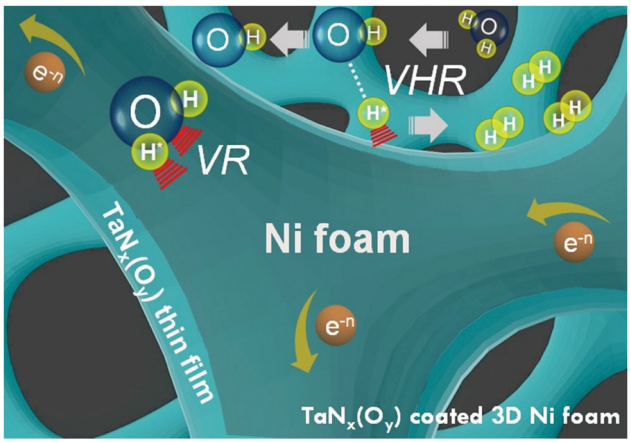

Fig. 4 Schematic representation of synergistic HER process involved in the surface of $TaN_x(O_y)$/NF catalysts [VR-Volmer reaction; VHR-Volmer–Heyrovsky reaction].

In conclusion, we have successfully demonstrated facile growth of tantalum-oxy nitride [$TaN_x(O_y)$] thin film on porous 3D nickel foam using ([$Ta(NEt)(NEt_2)_3$]) precursor *via* CVD as a novel self-supported catalyst for water splitting. Compared to bare NF, $TaN_x(O_y)$/NF displayed lower onset potential (−50 mV *vs.* −166 mV), lower Tafel slope (151 mV dec^{-1} *vs.* 179 mV dec^{-1}) and higher current density (−11.08 mA cm^{-2} *vs.* −3.36 mA cm^{-2} at 400 mV) for HER. This establishes the synergistic effect between $TaN_x(O_y)$/Ni coating for achieving enhanced HER performance.

The authors gratefully acknowledge financial assistance received through the Scheme for Promotion of Academic and Research Collaboration (SPARC), Department of Science and Technology (DST), Government of India (Project No.: SPARC/2018–2019/P781/SL; IITM Ref. No.: MET1819199SPARRAVK). The authors would also like to thank infrastructural support provided by University of Cologne, Germany. The funding received from the Institute of Eminence Research Initiative Project on Materials and Manufacturing for Futuristic Mobility (project no. SB20210850MMM HRD008275) is gratefully acknowledged.

Conflicts of interest

The authors declare that they have no conflict of interest.

References

1 F. Yu, L. Yu, I. K. Mishra, Y. Yu, Z. F. Ren and H. Q. Zhou, *Mater. Today Phys.*, 2018, 7, 121–138.
2 D. Zhang, J. Z. Soo, H. H. Tan, C. Jagadish, K. Catchpole and S. K. Karuturi, *Adv. Energy Sustainable Res.*, 2021, **2**, 2000071.
3 J. Theerthagiri, S. J. Lee, A. P. Murthy, J. Madhavan and M. Y. Choi, *Curr. Opin. Solid State Mater. Sci.*, 2020, **24**, 100805.
4 Y. Sun, T. Zhang, C. Li, K. Xu and Y. Li, *J. Mater. Chem. A*, 2020, **8**, 13415–13436.
5 Y. Abghoui and E. Skúlason, *J. Phys. Chem. C*, 2017, **121**, 24036–24045.
6 N. S. Alhajri, H. Yoshida, D. H. Anjum and A. T. Garcia-Esparza, *J. Mater. Chem. A*, 2013, 12606–12616.
7 F. Zhang, S. Xi, G. Lin, X. Hu, X. W. (David) Lou and K. Xie, *Adv. Mater.*, 2019, **31**, 1–7.
8 J. Kwon, H. S. Han, S. Choi, K. Park, S. Jo, U. Paik and T. Song, *ChemCatChem*, 2019, **11**, 5898–5912.
9 C. Li, B. Jiang, Z. Wang, Y. Li, M. S. A. Hossain, J. H. Kim, T. Takei, J. Henzie, Ö. Dag, Y. Bando and Y. Yamauchi, *Angew. Chem., Int. Ed.*, 2016, **55**, 12746–12750.
10 C. Li, M. Iqbal, J. Lin, X. Luo, B. Jiang, V. Malgras, K. C. W. Wu, J. Kim and Y. Yamauchi, *Acc. Chem. Res.*, 2018, **51**, 1764–1773.
11 C. Li, B. Jiang, N. Miyamoto, J. H. Kim, V. Malgras and Y. Yamauchi, *J. Am. Chem. Soc.*, 2015, **137**, 11558–11561.
12 H. Sun, Z. Yan, F. Liu, W. Xu, F. Cheng and J. Chen, *Adv. Mater.*, 2020, **32**, 1–18.
13 N. K. Chaudhari, H. Jin, B. Kim and K. Lee, *Nanoscale*, 2017, **9**, 12231–12247.
14 B. Liu, B. He, H. Q. Peng, Y. Zhao, J. Cheng, J. Xia, J. Shen, T. W. Ng, X. Meng, C. S. Lee and W. Zhang, *Adv. Sci.*, 2018, **5**, 1–7.
15 F. Song, W. Li, J. Yang, G. Han, P. Liao and Y. Sun, *Nat. Commun.*, 2018, **9**, 4531.
16 K. Sun, T. Zhang, L. Tan, D. Zhou, Y. Qian, X. Gao, F. Song, H. Bian, Z. Lu, J. Dang, H. Gao, J. Shaw, S. Chen, G. Chen and Y. Rao, *ACS Appl. Mater. Interfaces*, 2020, **12**, 29357–29364.
17 K. Lu, Y. Liu, F. Lin, I. A. Cordova, S. Gao, B. Li, B. Peng, H. Xu, J. Kaelin, D. Coliz, C. Wang, Y. Shao and Y. Cheng, *J. Am. Chem. Soc.*, 2020, **142**, 12613–12619.
18 J. Xie and Y. Xie, *ChemCatChem*, 2015, **7**, 2568–2580.
19 A. Ishihara, K. Lee, S. Doi, S. Mitsushima, N. Kamiya, M. Hara, K. Domen, K. Fukuda and K. I. Ota, *Electrochem. Solid-State Lett.*, 2005, 201–203.
20 F. van Steenbergen and A. Tuinhof, *Angew. Chem., Int. Ed.*, 2009, **40**, 1355–1360.
21 A. Kafizas, C. J. Carmalt and I. P. Parkin, *Coord. Chem. Rev.*, 2013, **257**, 2073–2119.
22 J.-g. Yang, Y.-l. Zhou and X. Guo-qiang, *Electrochemistry*, 2012, **80**, 26–29.
23 N. Arshi, J. Lu, Y. K. Joo, J. H. Yoon and B. H. Koo, *Surf. Interface Anal.*, 2015, **47**, 154–160.
24 Z. Wang, O. Yaegashi, H. Sakaue, T. Takahagi and S. Shingubara, *J. Appl. Phys.*, 2003, **94**, 4697–4701.
25 M. Chisaka, A. Ishihara, N. Uehara, M. Matsumoto, H. Imai and K. Ota, *J. Mater. Chem. A*, 2015, **3**, 16414–16418.
26 T. Shinagawa, A. T. Garcia-Esparza and K. Takanabe, *Sci. Rep.*, 2015, **5**, 1–21.
27 J. Lu, T. Xiong, W. Zhou, L. Yang, Z. Tang and S. Chen, *ACS Appl. Mater. Interfaces*, 2016, **8**, 5065–5069.
28 R. K. Singh, R. Ramesh, R. Devivaraprasad, A. Chakraborty and M. Neergat, *Electrochim. Acta*, 2016, **194**, 199–210.
29 A. B. Laursen, A. S. Varela, F. Dionigi, H. Fanchiu, C. Miller, O. L. Trinhammer, J. Rossmeisl and S. Dahl, *J. Chem. Educ.*, 2012, **89**, 1595–1599.
30 A. R. Zeradjanin, J. P. Grote, G. Polymeros and K. J. J. Mayrhofer, *Electroanalysis*, 2016, **28**, 2256–2269.